ACS OMEGA

Article

Cite This: ACS Omega 2019, 4, 15061−15066

http://pubs.acs.org/journal/acsodf

Fast and Efficient Sun Light Photocatalytic Activity of Au_ZnO Core−Shell Nanoparticles Prepared by a One-Pot Synthesis

Luca Spitaleri,[†] Giuseppe Nicotra,[‡] Massimo Zimbone,[§] Annalinda Contino,[†] Giuseppe Maccarrone,[†] Alessandra Alberti,[‡] and Antonino Gulino*[,†,∥]

[†]Department of Chemical Sciences, University of Catania, Viale Andrea Doria 6, 95125 Catania, Italy

[‡]CNR-IMM, Zona industriale Strada VIII, 5, 95121 Catania, Italy

[§]CNR-IMM, via S. Sofia 64, 95123 Catania, Italy

[∥]INSTM UdR of Catania, Viale Andrea Doria 6, 95125 Catania, Italy

Supporting Information

ABSTRACT: Gold nanostructures absorb visible light and show localized surface plasmon resonance bands in the visible region. Semiconducting ZnO nanostructures are excellent for ultraviolet detection, thanks to their wide band gap, large free exciton binding energy, and high electron mobility. Therefore, the coupling of gold and ZnO nanostructures represents the best-suited way to boost photodetection. With the above perspective, we report on the high photocatalytic activity of some Au_ZnO core−shell nanoparticles (NPs) recently prepared by a one-pot synthesis in which a [zinc citrate]$^-$ complex acted as the ZnO precursor, a reducing agent for Au^{3+}, and a capping anion for the obtained Au NPs. The overall nanostructures proved to be Au(111) NPs surrounded by a thin layer of [zinc citrate]$^-$ that evolved to Au_ZnO core−shell nanostructures. Worthy of note, with this photocatalyst, sun light efficiently decomposes a standard methylene blue solution according to ISO 10678:2010. We rationalized photodetection, reaction rate, and quantum efficiency.

INTRODUCTION

The need for clean water is fundamental to humanity. Typical wastewater management (filtration, chlorination, desalination, reverse osmosis, etc.) suffers from severe limitations because of the ineffective decontamination and/or elevated related costs. In this context, the peculiar properties of some new nanostructures may overcome these issues and promote unconventional water purification methods.

From this perspective, the ZnO-based photocatalyst has attracted great attention because of the low cost of ZnO and its excellent stability, abundance, and photoactivity. The main disadvantage of ZnO is its wide band gap that makes it promising for ultraviolet (UV) detection but less efficient for sun-driven applications. In fact, ZnO is a semiconductor with a wide band gap (3.37 eV), a large free exciton binding energy (60 meV), and a high electron mobility (~400 $cm^2\ V^{-1}\ s^{-1}$).[1,2]

However, noble-metal−ZnO composite nanostructures may overcome this problem as noble-metal nanoparticles (NPs) absorb visible light and generate localized surface plasmon resonances suitable to enhance photodetection of visible light.[3] Therefore, the conjugation of gold NPs and the wide band gap ZnO semiconductor is one of the most suitable ways to improve ultraviolet−visible (UV−vis) photodetection.[4−6]

In this context, there have been many reports concerning the photocatalytic activity of Au on ZnO materials, useful in many different technological fields.[7−22]

Conversely, a few studies of Au_ZnO having a core−shell structure (ZnO shell on Au NPs core) have been reported. Between them, the optical properties of ZnO shell grown on Ag and Au nanoparticle cores by a solution method have been investigated.[23] It was found that both ZnO/Ag and ZnO/Au show strongly enhanced near-band-edge UV exciton emission from the ZnO shells because of coupling with surface plasmon resonance of the metal NPs. These observations suggested the suitability of metal NPs for improving optical detection.

In another study, Au/ZnO core−shell NPs with different shell thicknesses were obtained by chemically depositing zinc oxide on gold NP surfaces.[24] A significant effect on the photoluminescence intensity and shortening of the decay time of the rhodamine 6G dye in the presence of Au/ZnO core−shell NPs was observed. The current−voltage curve of hybrid Au/ZnO exhibited a rectifying nature and represented the n-type Schottky diode behavior with a typical turn-on voltage between 0.6 and 1.3 V. It was also found that the rectifying ratio increases

Received: June 21, 2019
Accepted: August 6, 2019
Published: September 9, 2019

DOI: 10.1021/acsomega.9b01850
ACS Omega 2019, 4, 15061−15066

with decreasing thickness of the ZnO shell, whereas the electrical transport through the core−shell was similar to what was observed for pure ZnO sample NPs. Also, the nature of the O vacancy in graphitic-like ZnO bilayer films supported on Cu, Ag, and Au(111) surfaces was studied by quantum mechanical calculations.[25] Furthermore, hybrid semiconductor plasmonic nanostructures of zinc oxide on gold NPs were synthesized by the addition of ZnO quantum dots to a suspension of Au NPs of different sizes and so forth.[26]

Recently, we obtained some core−shell Au_ZnO NPs by reacting zinc citrate $Zn_3(C_6H_5O_7)_2{\cdot}2H_2O$ and $HAuCl_4{\cdot}3H_2O$ in a one-pot synthesis in which the [zinc citrate]$^-$ complex acted as the ZnO precursor, a reducing agent for Au^{3+}, and a capping anion for the obtained Au NPs.[6] Transmission electron microscopy (TEM) and energy dispersive X-ray (EDX) measurements provided evidence of Au(111) NPs with a mean radius of about 5 nm, surrounded by ∼2 nm layer of [zinc citrate]$^-$ that evolved in Au_$Zn(OH)_2$ and then in Au_ZnO.

Therefore, in the present investigation, we report on the photocatalytic activity of the above-mentioned Au_ZnO core−shell NPs, prepared by a one-pot synthesis, toward a standard methylene blue (MB) solution, according to ISO 10678:2010. Worthy of note, sun light was used as the irradiation source, and we observed a fast and efficient MB decomposition. Finally, we accurately calculated the number of adsorbed photons, the reaction rate, and the quantum efficiency.

RESULTS AND DISCUSSION

Semiconductor photocatalysts are a class of emerging nanomaterials that show many applications comprising the degradation of toxic pollutants. When the photocatalytic semiconductor is exposed to photons having energy equal to or higher than its band gap, the generated electron−hole pairs can react with atmospheric oxygen and produce highly reactive oxygen species suitable to promote oxidation processes for the degradation of many organic compounds. The coupling of surface plasmon resonance of Au NPs with the exciton emission in the ZnO shells induces enhanced absorption. With this aim, Au NPs (core) capped with ZnO (shell) were prepared in a single-step (one-pot) synthesis and characterized, and their photocatalytic behavior was exploited.[6]

XPS Results. The electronic study of the Au_ZnO nanostructure is fundamental to investigate the Au−ZnO electron interactions, which are the basis of the coupling of the plasmon Au resonance with the ZnO exciton emission, and X-ray photoelectron spectroscopy (XPS) represents the most suited tool to accomplish this task.[27,28] Figure 1a shows the XPS spectrum of Au_ZnO in the Au 4f−Zn 3p binding energy region. A careful deconvolution of this experimental profile reveals that the Au $4f_{7/2,5/2}$ spin−orbit components lie at 83.8 and 87.6 eV (3.8 eV spin−orbit coupling), thus indicating the presence of Au^0 states, usually expected at 84.0 eV ($4f_{7/2}$).[29] The Zn 3p spin−orbit components lie at 88.9 and 91.9 eV with a 3.0 eV spin−orbit coupling. These 3p levels are a couple of tens of eV at higher binding energy with respect to those previously reported for ZnO.[30]

Figure 1b shows the XPS of Au_ZnO in the Zn 2p binding energy region. The $2p_{3/2,1/2}$ spin−orbit components have been observed at 1023.7 and 1046.7 eV, respectively. These values are about 2 eV at higher energy with respect to typical values observed for pure ZnO materials[31−33] but almost identical to those previously reported for some Au−ZnO architectures.[34] This observation strongly confirms the electronic communication between ZnO and Au in a way that ZnO electrons are supplied to Au.

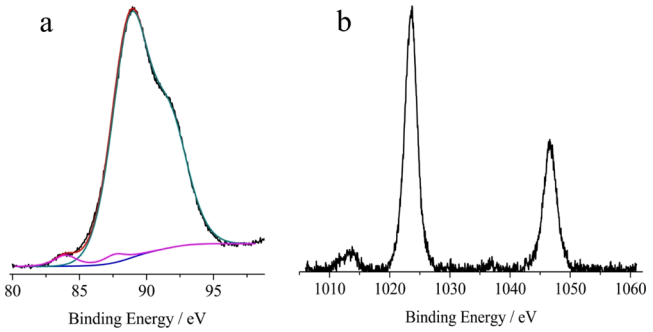

Figure 1. (a) Al Kα excited XPS of the Au_ZnO, dried at 130 °C, in the Au 4f−Zn 3p binding energy region. The black line refers to the experimental profile. The blue line represents the background; the magenta line refers to the Au 4f spin−orbit components; the green line refers to the Zn 3p spin−orbit components; the red line superimposed on the experimental profile refers to the sum of the Gaussian components. (b) Al Kα excited XPS of Au_ZnO, dried at 130 °C, in the Zn 2p binding energy region.

Finally, the XPS atomic concentration analysis revealed an Au/Zn percentage of 0.6, roughly corresponding to half of the nominal Au concentration. This result is acceptable since XPS probes only the surface of the Au_ZnO material whose composition is 98.5% in Zn.

TEM Measurements. TEM/scanning (STEM) microscopy (Figures 2, S1) shows the presence of NPs having a mean radius of about 5−10 nm. In addition, we noted that the Au NPs are oriented toward the (111) plane with the measured interplanar distance of 2.36 Å (Figure 2, right). EDX analyses clearly demonstrated that the experimental composition of the Au_ZnO nanostructures is identical to the nominal 1.5% of Au in ZnO (Figure S2).

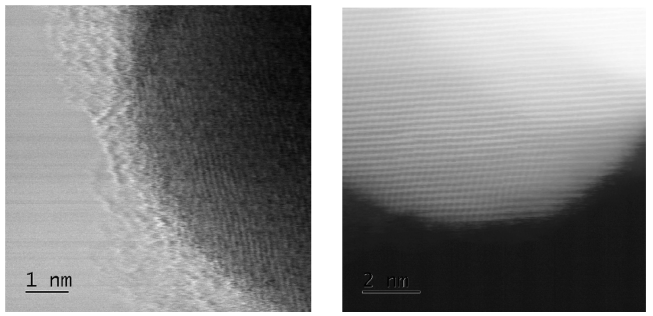

Figure 2. Left: Bright-field TEM showing a typical Au_ZnCit$^-$ NP having the core−shell structure. The dark area represents Au, and the surrounding shell represents the Zn complex; right: high-angle annular dark field-STEM at atomic resolution showing a representative Au NP highly oriented toward the (111) plane with an interplanar distance of 2.36 Å.

XRD Measurements. X-ray diffraction (XRD) measurements were performed on both ZnO and core−shell Au_ZnO samples. The obtained patterns, shown in Figure 3, have multiple contributions that have been attributed to different phases. The Au NPs provide clear and intense 111, 200, and 220 reflections of the face-centered cubic lattice with $Fm\bar{3}m$ symmetry (PDF 00-04-0784). Besides the gold contributions, the two patterns share common phases mostly ascribed to orthorhombic (PDF 00-020-1435) and tetragonal (PDF-00-

DOI: 10.1021/acsomega.9b01850
ACS Omega 2019, 4, 15061−15066

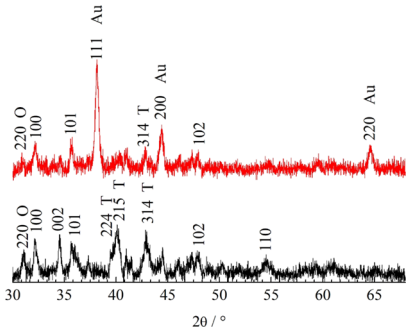

Figure 3. XRD patterns for ZnO (black line) and core−shell Au_ZnO (red line). The 100, 002, 102, 101, and 110 reflections belong to the ZnO hexagonal zincite structure. The 220 reflection belongs to the orthorhombic $Zn(OH)_2$ sweetite structure (indicated with the symbol O), whereas the 224, 215, and 314 reflections belongs to the tetragonal (indicated with the symbol T) $Zn(OH)_2$ sweetite structure.

38−0356) sweetite structures with stoichiometry $Zn(OH)_2$. The additional reflections 100, 002, and 102 (space group $P6_3mc$, COD ID 00-101-1258) and 101 and 110 (space group $P6_3mc$, PDF 01-075-1533) belong to the ZnO hexagonal zincite structure.

Optical Measurements. UV−vis experiments were performed by suspending 0.2 mg of ZnO or Au_ZnO in 3 mL of water. A small magnet was used to stir these solutions that remained clear during UV−vis measurements. The absorbance spectra (Figure 4) show a stronger absorption for the Au_ZnO

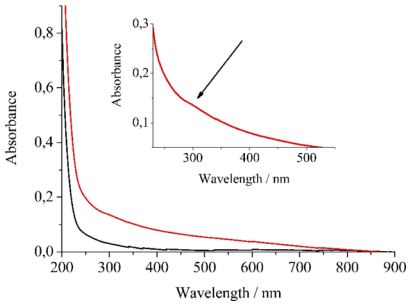

Figure 4. UV−vis absorption spectra of the water solutions obtained by suspending 0.2 mg of ZnO (black line) or Au_ZnO (red line) in 3 mL of water. These solutions have been stirred during UV−vis measurements. Inset: expanded scale of the UV−vis Au_ZnO absorption spectrum.

system with respect to the ZnO counterpart in the whole 200−900 nm range, and this is certainly due to the additional presence in the spectrum of Au_ZnO of the surface plasmon of the Au NPs. In fact, it is well known that the surface plasmon of Au NPs appears as a broad band peaked in the 500−600 nm wavelength region depending on their size and shape.[35−42] Thus, the absorption of the solution containing Au_ZnO is also due to the presence of the Au NP plasmon resonance, thus confirming that the coupling of Au NPs with ZnO enhanced the UV−vis photodetection.

Photocatalytic Experiments. Starting UV−vis spectra of the two aqueous solutions, each containing 3 mL of 1.44×10^{-5} M MB and 0.2 mg of ZnO or Au_ZnO powders, significantly differ in the wavelength region below 600 nm, since in the spectrum of the solution containing Au_ZnO, there is the presence of the Au NP plasmon resonance hidden under the MB absorbance band.

For both MB solutions, we observed an evident and monotonic absorbance decrease, consistent with the decomposition/decoloration of the dye (Figure 5a,b) upon irradiation. This evidence confirms the ability of both our oxides to act as efficient photocatalysts for water decontamination. A careful inspection of Figure 5a,b also indicates that Au_ZnO is more effective than ZnO, and this behavior is well evident in Figure 5c. In fact, Figure 5c shows that the MB concentration decreases as a function of the irradiation time for all samples with a first-order kinetic law. The curves were fitted in the range between 0 and 6 h with the following decreasing exponential formula: $\ln C/C_0 = -kt$, where k is the discoloration rate constant. The values of the discoloration rate obtained by using sun light are 0.566 and 0.712 h^{-1} (±0.01) for the MB solution in the presence of pure ZnO and core−shell Au_ZnO, respectively, with an increase of 26% in the latter case. These results are in agreement with the best, already reported, similar data for ZnO catalysts.[43]

The procedure to measure the efficiencies of MB decoloration for ZnO and Au_ZnO samples is described in the following. We started from the tabulated solar irradiance (Figure S3): the maximum sun irradiation is 1.32 $W/m^2/nm$ at 522 nm, and ∼0.86 $W/m^2/nm$ is observed at both 400 and 800 nm visible limits. Integrating in the 300−2500 nm wavelength range, the solar intensity is calculated to be 830 W/m^2 (less than 1 kW/m^2). Nevertheless, during our discoloration experiments, we measured an integrated irradiance of 70 mW/cm^2 = 700 W/m^2, about 84% of the total tabulated sun irradiance (integrated over 300−2500 nm). In order to calculate the solar spectrum hitting the sample during our experiment, we rescaled the tabulated spectra, taking into account the effective measured intensity. Dividing this solar spectral irradiation by the photon energy at each wavelength and taking into account the exposed surface of the cuvette, we are able to calculate the number of photons/m^2·nm·s (N) hitting our cuvette. The number of photons adsorbed (N_{ass}) by the oxides is calculated by using the formula $N_{ass} = N \cdot (1 - 10^{-absorbance})$, where the absorbance spectra are reported in Figure 4 (absorbance of ZnO or Au_ZnO). The number of absorbed photons/m^2·nm·s is showed in Figure 6 at each wavelength.

According to the absorbance spectra reported in Figure 4 and in agreement with our expectation, Au_ZnO (pale gray) absorbs an order of magnitude more photons than ZnO (white) itself. The total number of photons/m^2·nm·s between 300 and 2500 nm is calculated by integrating the curves showed in Figure 6 and are reported in Figure S4. The quartz cuvette contained 3 mL of 1.44×10^{-5} M (2.60×10^{16} MB molecules) water solutions of MB, and only one side of it was exposed to sunlight so that the total exposed surface was 3 cm^2. Therefore, after 4 h of solar irradiation (14 400 s), 9.9×10^{19} and 5.7×10^{20} photons are absorbed by each solution, containing ZnO or Au_ZnO, respectively. By using the data of Figure 5a,b, after 4 h, 2.34×10^{16} and 2.45×10^{16} MB molecules were decomposed by ZnO and Au_ZnO, respectively. By dividing each of these values by the appropriate number of absorbed photons ($2.34 \times 10^{16}/9.9 \times 10^{19} \times 100$ = 0.024% and $2.45 \times 10^{16}/5.7 \times 10^{20} \times 100$ = 0.0043%), we got the quantum efficiency values for the two catalysts (0.024% for ZnO and 0.0043% for Au_ZnO). Therefore, it is evident that Au_ZnO, with respect to ZnO itself, shows an order of magnitude increased absorption (5.7×10^{20}), 26% increased discoloration rate (0.712 h^{-1}), and nevertheless lower quantum efficiency (0.0043%).

Concerning the MB photodegradation mechanism, the irradiation of a semiconductor moves electrons from the valence

DOI: 10.1021/acsomega.9b01850
ACS Omega 2019, 4, 15061−15066

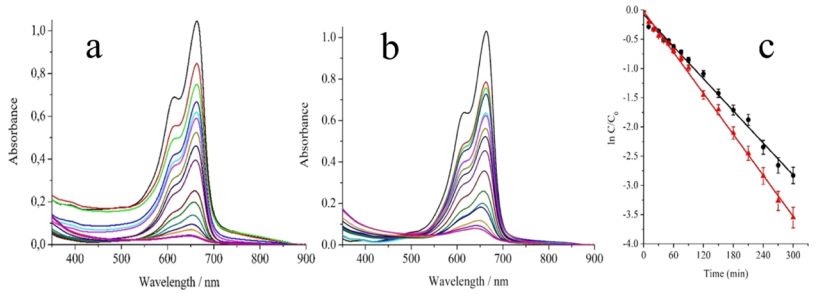

Figure 5. (a) Absorbance spectra for 1.44×10^{-5} M water solution of MB exposed to different solar light irradiation times in the presence of ZnO. The black, red, green, blue, cyan, magenta, dark yellow, navy, purple, wine, olive, dark cyan, royal, orange, violet, and pink lines refer to the starting MB solution at 0, 10, 20, 30, 40, 50, 60, 75, 90, 120, 150, 180, 210, 240, 270, and 300 min irradiation time, respectively. (b) Absorbance spectra for a 1.44×10^{-5} M water solution of MB, exposed to different solar light irradiation times in the presence of Au_ZnO. The black, red, green, blue, cyan, magenta, dark yellow, navy, purple, wine, olive, dark cyan, royal, orange, violet, and pink lines refer to the starting MB solution at 0, 10, 20, 30, 40, 50, 60, 75, 90, 120, 150, 180, 210, 240, 270, and 300 min irradiation time, respectively. (c) Integrated rate behavior for first-order reaction kinetics obtained from absorbance measured at 662.2 nm (band maximum) for 1.44×10^{-5} M water solutions of MB exposed to solar light. Black and red lines are related to the MB with pure ZnO and Au_ZnO, respectively. In both cases, the fit goodness was 99%.

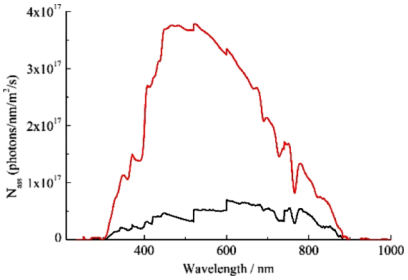

Figure 6. Calculated absorbed solar photons for ZnO (black line) and Au_ZnO (red line) catalysts.

to conduction band. The excited electrons and the resulting holes have strong reductive and oxidative powers, respectively, and produce reactive oxygen species. In this context, it has already been reported that the energy edges of valence and conduction bands of semiconductors determine the type of generated reactive oxygen species.[21] Thus, in ZnO, holes react with water to produce hydroxyl radicals, and electrons react with dissolved oxygen to yield superoxide anions. Moreover, superoxide anions can react with holes to form singlet oxygen during irradiation of ZnO/Au NPs. The reaction of MB with these reactive oxygen species results in *N*-demethylation of its auxochromic dimethylamine groups plus water and carbon dioxide.

In general, photoactivity is a rather complex behavior that involves several steps: (i) generation of the electron−hole pairs (related to photon absorption), (ii) separation and diffusion of the charge carriers to the active surface sites, (iii) reaction of holes with defects or with the MB on the surface-solution interphase, and (iv) electron scavenging. Therefore, the observed different quantum efficiencies could be due to the different lifetimes of the electron−hole pairs generated by the photons impinging on the two ZnO and Au_ZnO catalysts. The inset reported in Figure 4 shows the expanded scale of the absorbance spectrum of Au_ZnO and clearly indicates a small but significant feature at about 300 nm, consistent with the presence of states in the band gap, absent in the present ZnO system.

It is important to mention that our present study does not really allow to recognize the nature of compensating defects as cation vacancies, interstitial oxygen, or more complex defect clusters.[44] Nevertheless, it has already been reported that some defect states associated with the presence of zinc hydroxide $Zn(OH)_2$ layers on the surface of ZnO nanocrystallites should enhance the photocatalytic activity, and by XRD measurements, we revealed some $Zn(OH)_2$ in the Au_ZnO core−shell NPs.[45,46]

In addition, we cannot exclude the role of other defects at the grain boundaries as partially responsible for the lower quantum efficiency found using the present Au_ZnO catalyst. In fact, it could also be possible due to the presence of a few Au^{3+} ions as dopants that substitute for Zn^{2+} in the zincite ZnO structure. In this case, the extra electron provided by Au^{3+} could go in the 4s−4p hybrid empty conduction band or, more likely, form a localized state deep in the band gap, as it seems evident in the inset of Figure 4. These states could be traps for the electrons of the electron−hole pair and be responsible for the decreased quantum efficiency of the Au_ZnO catalyst.

CONCLUSIONS

In the present study, the UV−vis photodetection of ZnO was enhanced by about 1 order of magnitude by obtaining Au_ZnO core−shell nanostructures, prepared by a one-pot synthesis in which the $[\text{zinc citrate}]^-$ complex acted as the ZnO precursor, a reducing agent for Au^{3+}, and a capping anion for the obtained Au(111) NPs. An increased absorption was observed in Au_ZnO because of the additional presence of the surface plasmon resonance of the Au NPs. As already reported for similar systems, electronic interactions between gold and n-type semiconductor ZnO at their interfaces allows the generation of superoxide species.[15] In fact, using this Au_ZnO photocatalyst, sun light efficiently decomposes a standard MB solution, according to ISO 10678:2010, with a better photocatalytic activity (increased of 26%) than that observed using ZnO, even though the decomposition rate did not increase by an order of magnitude because of the lower quantum efficiency observed for the Au_ZnO system.

EXPERIMENTAL DETAILS

Synthesis of Au_ZnO Core−Shell NPs. The synthesis of Au NPs capped with ZnO NPs was performed as previously reported.[6] In particular, an appropriate quantity of zinc citrate $Zn_3(C_6H_5O_7)_2{\cdot}2H_2O$ [hereafter $Zn_3(Cit)_2$] was introduced into a three-necked flask and kept in the refrigerator at 5 °C. After 1 day, the mixture was totally clear (zinc citrate is more soluble in cold water than in warm water), and the measured pH was 6.50.

DOI: 10.1021/acsomega.9b01850
ACS Omega 2019, 4, 15061−15066

Then, we brought this solution on a heating plate and slowly added aliquots of a $HAuCl_4 \cdot 3H_2O$ solution in order to have a final 1.5% Au^{3+} concentration in Zn^{2+}. Then, the solution was left to cool, thus leaving Au NPs as a consequence of the reducing power of the $[ZnCit]^-$ complex.[6] Afterward, we dropwise added conc. NH_3 to obtain a white gel of Au_Zn-$(OH)_2$ at pH = 8.9. Finally, the overall gel was dialyzed with deionized water, left to evaporate up to a few mL, and dried at 130 °C. A similar synthetic procedure was used to synthesize ZnO without any addition of $HAuCl_4 \cdot 3H_2O$. In the present study, we are dealing with ZnO and Au_ZnO dried at 130 °C since the photocatalytic behavior of the materials obtained at this temperature is better than that observed for the same materials sintered at higher temperatures (up to 1000 °C). At this temperature (130 °C), we observed the presence of some hydrated ZnO (vide infra), but for convenience, we will refer to ZnO throughout the paper.

TEM Measurements. TEM measurements were performed by means of a JEOL ARM200F atomic resolution analytical microscope. A Cu/C TEM grid represented the sample holder. A 60 K eV electron beam was used for STEM and EDX analyses.

X-ray Photoelectron Data. XPS spectra were collected with a PHI 5600 instrument (base pressure of the main chamber 3×10^{-8} Pa) using the Al Kα X-ray radiation and a pass energy of 5.85 eV.[27,28] Under these conditions, the instrumental energy resolution was better than 0.5 eV. Al Kα X-ray satellite structures were subtracted before to process the data. A Shirley background was removed from the XPS peaks. The main C 1s peak at 285.0 eV was used to calibrate the spectra.[27] XPS was performed on samples dried at 130 °C. The instrumental atomic sensitivity factors were used to get the atomic concentration analysis. The fitting of the Au 4f−Zn 3p spectrum was performed with symmetrical Gaussian envelopes.

XRD Analysis. XRD data were obtained with a D8 Discover Bruker AXS diffractometer (Cu Kα source) equipped with soller silts and operating in 2θ−Ω geometry. The patterns were acquired with a 0.01° step size and a step time of 10 s/step. The powder compounds were pelletized between tungsten carbide dies at 500 kg/cm and then loaded on the sample holder.

UV−Vis Spectra. UV−vis data were obtained using a UV−vis V-650 Jasco spectrometer at 0.2 nm resolution at room temperature.

pH was measured with a standardized Metrohm E 654 glass microelectrode (pH uncertainty = ± 0.01).

Photocatalytic Behavior. Photocatalysis experiments were performed using two quartz cuvettes, each containing 3 mL of 1.44×10^{-5} M MB aqueous solution, in which we added 0.2 mg of ZnO or Au_ZnO powders. The cuvettes were covered with lids to preclude solvent evaporation during the experiment and left in the dark for 60 min to permit the adsorption of the dye on the oxides to reach equilibrium. The measured pH of both solutions was 7.6. UV−vis spectra before and after being in the dark for 60 min were identical. Then, we added a small magnetic stir bar in each solution, placed them on a magnetic stirrer, and left them covered with lids under the sun light for up to 300 min. The solar irradiation, measured using a Thorlabs power meter was 70 mW/cm^2. Initially, the cuvette solutions were subjected to fast UV−vis absorbance measurements after cycles of 10 min irradiation. After 90 min of sun light irradiation, UV−vis measurements were performed every 30 min.

■ ASSOCIATED CONTENT

Supporting Information

The Supporting Information is available free of charge on the ACS Publications website at DOI: 10.1021/acsomega.9b01850.

TEM and EDX of the core−shell Au_ZnO NPs; solar irradiance in the 300−2500 wavelength range; and integrated absorbed photons in the 300−2500 nm range for ZnO and Au_ZnO catalysts (PDF)

■ AUTHOR INFORMATION

Corresponding Author

*E-mail: agulino@unict.it. Phone: +39-095-7385067. Fax. +39-095-580138.

ORCID

Alessandra Alberti: 0000-0002-4103-6208

Antonino Gulino: 0000-0002-6850-3080

Author Contributions

The manuscript was written through contributions of all authors. All authors have given approval to the final version of the manuscript.

Notes

The authors declare no competing financial interest.

■ ACKNOWLEDGMENTS

The authors thank the University of Catania for (Piano della Ricerca di Ateneo 2016−2018) the financial support.

■ REFERENCES

(1) Zhang, Z.; Choi, M.; Baek, M.; Deng, Z.; Yong, K. Corrosion-assisted self-growth of Au-decorated ZnO corn silks and their photoelectrochemical enhancement. *ACS Appl. Mater. Interfaces* **2017**, *9*, 3967−3976.

(2) Xu, S.; Wang, Z. L. One-dimensional ZnO nanostructures: solution growth and functional properties. *Nano Res.* **2011**, *4*, 1013−1098.

(3) Anker, J. N.; Hall, W. P.; Lyandres, O.; Shah, N. C.; Zhao, J.; Van Duyne, R. P. Biosensing with plasmonic nanosensors. *Nat. Mater.* **2008**, *7*, 442−453.

(4) Liu, X.; Iocozzia, J.; Wang, Y.; Cui, X.; Chen, Y.; Zhao, S.; Li, Z.; Lin, Z. Noble metal-metal oxide nanohybrids with tailored nanostructures for efficient solar energy conversion, photocatalysis and environmental remediation. *Energy Environ. Sci.* **2017**, *10*, 402−434.

(5) Rodriguez, J. A.; Senanayake, S. D.; Stacchiola, D.; Liu, P.; Hrbek, J. The activation of gold and the water-gas shift reaction: Insights from studies with model catalysts. *Acc. Chem. Res.* **2014**, *47*, 773−782.

(6) Contino, A.; Maccarrone, G.; Spitaleri, L.; Torrisi, L.; Nicotra, G.; Gulino, A. One Pot Synthesis of Au_ZnO Core-Shell Nanoparticles Using a Zn Complex Acting as ZnO Precursor, Capping and Reducing Agent During the Formation of Au NPs. *Eur. J. Inorg. Chem.* **2018**, *2018*, 4678−4683.

(7) Thang, H. V.; Pacchioni, G. Spontaneous Formation of Gold Cluster Anions on ZnO/Cu(111) Bilayer Films. *J. Phys. Chem. C* **2019**, *123*, 7644−7653.

(8) Cure, J.; Assi, H.; Cocq, K.; Marìn, L.; Fajerwerg, K.; Fau, P.; Bêche, E.; Chabal, Y. J.; Estève, A.; Rossi, C. Controlled Growth and Grafting of High-Density Au Nanoparticles on Zinc Oxide Thin Films by Photo-Deposition. *Langmuir* **2018**, *34*, 1932−1940.

(9) She, P.; Xu, K.; Yin, S.; Shang, Y.; He, Q.; Zeng, S.; Sun, H.; Liu, Z. Bioinspired self-standing macroporous Au/ZnO sponges for enhanced photocatalysis. *J. Colloid Interface Sci.* **2018**, *514*, 40−48.

(10) Zhang, Y.; Zhou, J.; Li, Z.; Feng, Q. Photodegradation pathway of rhodamine B with novel Au nanorods @ ZnO microspheres driven by visible light irradiation. *J. Mater. Sci.* **2018**, *53*, 3149−3162.

DOI: 10.1021/acsomega.9b01850
ACS Omega 2019, 4, 15061−15066

(11) She, P.; Xu, K.; Shang, Y.; He, Q.; Zeng, S.; Yin, S.; Lu, G.; Liang, S.; Sun, H.; Liu, Z.; Liu, Z. ZnO nanodisks decorated with Au nanorods for enhanced photocurrent generation and photocatalytic activity. *New J. Chem.* **2018**, *42*, 3315−3321.
(12) Choudhary, M. K.; Kataria, J.; Sharma, S. Novel Green Biomimetic Approach for Preparation of Highly Stable Au-ZnO Heterojunctions with Enhanced Photocatalytic Activity. *ACS Appl. Nano Mater.* **2018**, *1*, 1870−1878.
(13) Jiang, X.; He, W.; Zhang, X.; Wu, Y.; Zhang, Q.; Cao, G.; Zhang, H.; Zheng, J.; Croley, T. R.; Yin, J.-J. Light-Induced Assembly of Metal Nanoparticles on ZnO Enhances the Generation of Charge Carriers, Reactive Oxygen Species, and Antibacterial Activity. *J. Phys. Chem. C* **2018**, *122*, 29414−29425.
(14) Fernando, J. F. S.; Shortell, M. P.; Firestein, K. L.; Zhang, C.; Larionov, K. V.; Popov, Z. I.; Sorokin, P. B.; Bourgeois, L.; Waclawik, E. R.; Golberg, D. V. Photocatalysis with Pt-Au-ZnO and Au-ZnO Hybrids: Effect of Charge Accumulation and Discharge Properties of Metal Nanoparticles. *Langmuir* **2018**, *34*, 7334−7345.
(15) Corro, G.; Cebada, S.; Pal, U.; Fierro, J. L. G. Au^0-Au^{3+} bifunctional site mediated enhanced catalytic activity of Au/ZnO composite in diesel particulate matter oxidation. *J. Catal.* **2017**, *347*, 148−156.
(16) Bao, Z.; Yuan, Y.; Leng, C.; Li, L.; Zhao, K.; Sun, Z. One-pot synthesis of noble metal/zinc oxide composites with controllable morphology and high catalytic performance. *ACS Appl. Mater. Interfaces* **2017**, *9*, 16417−16425.
(17) Wei, R.-B.; Kuang, P.-Y.; Cheng, H.; Chen, Y.-B.; Long, J.-Y.; Zhang, M.-Y.; Liu, Z.-Q. Plasmon-Enhanced Photoelectrochemical Water Splitting on Gold Nanoparticle Decorated ZnO/CdS Nanotube Arrays. *ACS Sustainable Chem. Eng.* **2017**, *5*, 4249−4257.
(18) Han, N. S.; Kim, D.; Lee, J. W.; Kim, J.; Shim, H. S.; Lee, Y.; Lee, D.; Song, J. K. Unexpected Size Effect Observed in ZnO-Au Composite Photocatalysts. *ACS Appl. Mater. Interfaces* **2016**, *8*, 1067−1072.
(19) Mikami, G.; Grosu, F.; Kawamura, S.; Yoshida, Y.; Carja, G.; Izumi, Y. Harnessing self-supported Au nanoparticles on layered double hydroxides comprising Zn and Al for enhanced phenol decomposition under solar light. *Appl. Catal., B* **2016**, *199*, 260−271.
(20) Lin, W.-H.; Chiu, Y.-H.; Shao, P.-W.; Hsu, Y.-J. Metal-Particle-Decorated ZnO Nanocrystals: Photocatalysis and Charge Dynamics. *ACS Appl. Mater. Interfaces* **2016**, *8*, 32754−32763.
(21) He, W.; Kim, H.-K.; Wamer, W. G.; Melka, D.; Callahan, J. H.; Yin, J.-J. Photogenerated charge carriers and reactive oxygen species in ZnO/Au hybrid nanostructures with enhanced photocatalytic and antibacterial activity. *J. Am. Chem. Soc.* **2014**, *136*, 750−757.
(22) Yang, T.-H.; Huang, L.-D.; Harn, Y.-W.; Lin, C.-C.; Chang, J.-K.; Wu, C.-I.; Wu, J.-M. High density unaggregated Au nanoparticles on ZnO nanorod arrays function as efficient and recyclable photocatalysts for environmental purification. *Small* **2013**, *9*, 3169−3182.
(23) Guidelli, E. J.; Baffa, O.; Clarke, D. R. Enhanced UV Emission From Silver/ZnO And Gold/ZnO Core-Shell Nanoparticles: Photoluminescence, Radioluminescence, And Optically Stimulated Luminescence. *Sci. Rep.* **2015**, *5*, 14004.
(24) Haldar, K. K.; Sen, T. Shell thickness matters! Energy transfer and rectification study of Au/ZnO core/shell nanoparticles. *J. Colloid Interface Sci.* **2016**, *484*, 263−269.
(25) Thang, H. V.; Pacchioni, G. Oxygen Vacancy in Wurtzite ZnO and Metal-Supported ZnO/M(111) Bilayer Films (M = Cu, Ag and Au). *J. Phys. Chem. C* **2018**, *122*, 20880−20887.
(26) Rahman, D. S.; Ghosh, S. K. Manipulating Electron Transfer in Hybrid ZnO-Au Nanostructures: Size of Gold Matters. *J. Phys. Chem. C* **2016**, *120*, 14906−14917.
(27) Briggs, D.; Grant, J. T. *Surface Analysis by Auger and X-ray Photoelectron Spectroscopy*; IMP: Chichester, UK, 2003.
(28) Gulino, A. Structural and electronic characterization of self-assembled molecular nanoarchitectures by X-ray photoelectron spectroscopy. *Anal. Bioanal. Chem.* **2013**, *405*, 1479−1495.
(29) Kanehara, M.; Takahashi, H.; Teranishi, T. Gold(0) Porphyrins on Gold Nanoparticles. *Angew. Chem., Int. Ed.* **2008**, *47*, 307−310; *Angew. Chem.* **2008**, *120*, 313−316.
(30) Schön, G. Auger and direct electron spectra in X-ray photoelectron studies of zinc, zinc oxide, gallium and gallium oxide. *J. Electron Spectrosc. Relat. Phenom.* **1973**, *2*, 75.
(31) Gulino, A.; Lupo, F.; Fragalà, M. E. Substrate-free, self-standing ZnO thin films. *J. Phys. Chem. C* **2008**, *112*, 13869−13872.
(32) Gulino, A.; Dapporto, P.; Rossi, P.; Fragalà, I. Synthesis and characterization of liquid MOCVD precursors for thin films of cadmium oxide. *Chem. Mater.* **2002**, *14*, 4955−4962.
(33) Gulino, A.; Fragala, I. Deposition and characterization of transparent thin films of zinc oxide doped with Bi and Sb. *Chem. Mater.* **2002**, *14*, 116−121.
(34) Arunkumar, S.; Hou, T.; Kim, Y.-B.; Choi, B.; Park, S. H.; Jung, S.; Lee, D.-W. Au decorated ZnO hierarchical architectures: facile synthesis, tunable morphology and enhanced CO detection at room temperature. *Sens. Actuators, B* **2017**, *243*, 990−1001.
(35) Prasad, B. L. V.; Sorensen, C. M.; Klabunde, K. J. Gold nanoparticle superlattices. *Chem. Soc. Rev.* **2008**, *37*, 1871−1883.
(36) Shevchenko, E. V.; Talapin, D. V.; Kotov, N. A.; O'Brien, S.; Murray, C. B. Structural diversity in binary nanoparticle superlattices. *Nature* **2006**, *439*, 55−59.
(37) Macfarlane, R. J.; Lee, B.; Jones, M. R.; Harris, N.; Schatz, G. C.; Mirkin, C. A. Nanoparticle superlattice engineering with DNA. *Science* **2011**, *334*, 204−208.
(38) Kalsin, A. M.; Fialkowski, M.; Paszewski, M.; Smoukov, S. K.; Bishop, K. J. M.; Grzybowski, B. A. Electrostatic self-assembly of binary nanoparticle crystals with a diamond-like lattice. *Science* **2006**, *312*, 420−424.
(39) Jones, M. R.; Osberg, K. D.; Macfarlane, R. J.; Langille, M. R.; Mirkin, C. A. Templated techniques for the synthesis and assembly of plasmonic nanostructures. *Chem. Rev.* **2011**, *111*, 3736−3827.
(40) Manna, L.; Milliron, D. J.; Meisel, A.; Scher, E. C.; Alivisatos, A. P. Controlled growth of tetrapod-branched inorganic nanocrystals. *Nat. Mater.* **2003**, *2*, 382−385.
(41) Yin, Y.; Alivisatos, A. P. Colloidal nanocrystal synthesis and the organic-inorganic interface. *Nature* **2005**, *437*, 664−670.
(42) Contino, A.; Maccarrone, G.; Fragalà, M. E.; Spitaleri, L.; Gulino, A. Conjugated Gold-Porphyrin Monolayers Assembled on Inorganic Surfaces. *Chem.—Eur. J.* **2017**, *23*, 14937−14943.
(43) Zimbone, M.; Cacciato, G.; Boutinguiza, M.; Gulino, A.; Cantarella, M.; Privitera, V.; Grimaldi, M. G. Hydrogenated black-TiO_x: A facile and scalable synthesis for environmental water purification. *Catal. Today* **2019**, *321-322*, 146−157.
(44) Gulino, A.; Taverner, A. E.; Warren, S.; Harris, P.; Egdell, R. G. A photoemission study of Sb-doped TiO_2. *Surf. Sci.* **1994**, *315*, 351−361.
(45) Wu, J. M.; Chen, Y.-R. Ultraviolet-Light-Assisted Formation of ZnO Nanowires in Ambient Air: Comparison of Photoresponsive and Photocatalytic Activities in Zinc Hydroxide. *J. Phys. Chem. C* **2011**, *115*, 2235−2243.
(46) Bohle, D. S.; Spina, C. J. The Relationship of Oxygen Binding and Peroxide Sites and the Fluorescent Properties of Zinc Oxide Semiconductor Nanocrystals. *J. Am. Chem. Soc.* **2007**, *129*, 12380−12381.

DOI: 10.1021/acsomega.9b01850
ACS Omega 2019, 4, 15061−15066